4A.2 RAPID-SCAN, DUAL-POLARIZATION RADAR OBSERVATIONS OF TORNADIC AND NONTORNADIC MESOCYCLONES IN THE CONTEXT OF FORECASTER CONCEPTUAL MODELS

Charles M. Kuster*[1,3] and Pamela L. Heinselman[2,3]

[1]Cooperative Institute for Mesoscale Meteorological Studies, [2]NOAA/OAR National Severe Storms Laboratory, [3]University of Oklahoma, Norman, Oklahoma

ABSTRACT

On 31 May 2013, multiple supercells occurred near El Reno, Oklahoma. The first supercell produced two tornadoes including a long-track EF3, while the second supercell produced one brief EF0 tornado. Both of these storms were sampled by a research dual-polarization Weather Surveillance Radar-1988 Doppler (WSR-88D) located in Norman, Oklahoma (KOUN). Radar operators used a specialized volume coverage pattern with 10 elevation angles and 90° sector scans, which resulted in volumetric update times of about 1.6 min. At the same time, the nearby National Weather Radar Testbed Phased Array Radar collected one-min volume scans of the same storms. Using this unique dataset, we quantified the evolution of four dual-polarization supercell signatures (Z_{DR} column, Z_{DR} arc, K_{DP} column, K_{DP} foot) for both storms and compared this evolution to the evolution of features typically used by National Weather Service forecasters while issuing tornado warnings (e.g., mesocyclone intensity). Our analysis of the dual-polarization signatures revealed no clear precursors for tornadogenesis or patterns relative to mesocyclone or inflow evolution in this case. Relative maxima in the signatures' magnitude occurred prior to, during, and after the development of tornadic and nontornadic mesocyclones in this case. Relative maxima in Z_{DR} column size and magnitude did occur about 8–10 min prior to large hail reports, however. This pattern provides additional evidence that Z_{DR} columns provide information about updraft strength and could act as precursors for increased precipitation intensity at the surface.

1. INTRODUCTION

To better understand and anticipate threats posed by severe convective storms, National Weather Service (NWS) forecasters use conceptual models to increase their situational awareness (e.g., Doswell and Burgess 1993; Andra et al. 2002). As understanding of meteorological phenomenon increases and new technology becomes available, it is important to refine and add to these conceptual models (e.g., Andra et al. 2002). The completion of the dual-polarization upgrade to the Weather Surveillance Radar-1988 Doppler (WSR-88D) network in 2013 provides one such opportunity for adding to conceptual models since a new set of radar products became available to NWS forecasters (NOAA 2013).

Prior to this upgrade, researchers were using data from dual-polarization research radars to examine signatures within the dual-polarization variables (e.g., Wakimoto and Bringi 1988; Zrnić et al. 1993; Kumjian and Ryzhkov 2008). Several studies examined dual-polarization signatures frequently observed with supercells and how these signatures evolved relative to supercell evolution and tornadogenesis (e.g., Romine et al. 2008; Van Den Broeke et al. 2008; Kumjian et al. 2010). In a study of 14 supercells using dual-polarization radar data, Kumjian and Ryzhkov (2008) noted an elongated area of very high differential reflectivity (Z_{DR}) at the low levels (below 2 km) along the forward flank high reflectivity gradient. They called this signature the Z_{DR} arc and suggested that it formed as a result of hydrometeor size sorting caused by environmental wind shear. Later studies (e.g., Dawson et al. 2015) also supported this hypothesis. Since the signature is likely associated with enhanced wind shear, it can indicate that a given storm or portion of a quasi-linear convective system (QLCS) may pose a greater tornado threat (e.g., Mahale et al. 2012; Kumjian 2013). Kumjian and Ryzhkov (2008) also noted the presence of midlevel Z_{DR} half rings or rings. This distortion of the Z_{DR} column (e.g., Conway and Zrnić 1993) resulted from midlevel vorticity associated with the supercell's mesocyclone. Through a study of a nontornadic supercell with rapid-scan dual-polarization data collected by a research WSR-88D in Norman, OK (KOUN), Kumjian et al. (2010) noted that a full ring was present during the mesocyclone's mature stage, which later dissipated as the mesocyclone occluded.

Earlier studies using radar and aircraft measurements have also identified a column of enhanced specific differential phase (K_{DP}) within thunderstorms and called it the K_{DP} column (Hubbert et al. 1998; Loney et al. 2002). Loney et al. (2002) as

*Corresponding author address: Charles M. Kuster, National Weather Center, 120 David L. Boren Blvd., Norman, OK, 73072. E-mail: charles.kuster@noaa.gov

well as other radar-based studies of supercells (e.g., Kumjian and Ryzhkov 2008; Romine et al. 2008) noted that K_{DP} column location was offset from Z_{DR} column location in supercells potentially due to environmental wind shear. Romine et al. (2008) also discussed the low-level continuation of the K_{DP} column, which they called the K_{DP} foot (also referred to as "K_{DP} shield" in Crowe et al. 2012). In their study of a tornadic supercell, the K_{DP} foot was an elongated area of high K_{DP} located within the forward flank downdraft. They also observed that the maximum K_{DP} within this signature shifted towards the forward-left edge of the Z_{DR} arc prior to tornadogenesis. Crowe et al. (2012) studied multiple tornadic thunderstorms in northern Alabama and showed that there was more separation (i.e., less overlap) between the K_{DP} foot and Z_{DR} arc while the storm was producing a tornado as opposed to when the storm was not producing a tornado.

Previous studies have noted the existence of dual-polarization supercell signatures and have performed qualitative and some quantitative assessments of their evolution relative to tornadogenesis, yet uncertainty remains with regards to whether or not these signatures provide precursors to tornadogenesis. There is also uncertainty in how dual-polarization signatures relate to features typically used by NWS forecasters while issuing tornado warnings (e.g., mesocyclone evolution; inflow evolution), so more quantitative work is needed (e.g., Kumjian et al. 2008; Van Den Broeke et al. 2008). Therefore, the purpose of this study is to quantitatively examine the evolution of dual-polarization supercell signatures using rapid-update radar data to explore any potential connections with features that forecasters typically use while issuing tornado warnings. To accomplish this objective, we analyzed the evolution of dual-polarization signatures associated with tornadic and nontornadic mesocyclones within two supercells—one producing a strong long-track tornado and the other producing a weak short-lived tornado—occurring on 31 May 2013 in central Oklahoma. The evolution of dual-polarization supercell signatures is also compared with the evolution of low-level mesocyclone and inflow intensity. In this study, We are not investigating what the evolution of dual-polarization signatures might reveal about tornadogenesis, but rather are looking at whether or not this evolution can aid forecasters in anticipating imminent changes in mesocyclone intensity and tornadogenesis.

2. RADAR DATA

We used data from two radars nearly colocated in Norman, OK to analyze signatures on 31 May 2013. Dual-polarization signature evolution was quantified using KOUN data, while mesocyclone and inflow evolution was quantified using the National Weather Radar Testbed Phased Array Radar (NWRT PAR; hereafter PAR) data due to its faster volumetric update time (Table 1). KOUN transmits at a wavelength of 11.09 cm (S-band) and has an effective beamwidth of 1.06°. On 31 May 2013, KOUN radar operators used special 90° sector scans containing 10 elevation angles, which produced a volumetric update time of about 1.6 min. PAR transmits at a wavelength of 9.38 cm (S-band) and has a transmit beamwidth of 1.5° at boresight that increases to 2.1° at ± 45° from boresight. The radar electronically scans a 90° sector and provides volumetric update times of about one min. On 31 May 2013, radar operators used a modified VCP 12 (Brown et al. 2005) that contained five additional elevation angles up to 52.9°.

3. EVENT OVERVIEW

Environmental conditions on 31 May 2013 appeared favorable for strong supercells capable of producing long-track tornadoes. An analysis of the special sounding launched from Norman, OK at 1800 UTC (Fig. 1a) revealed steep low- and midlevel lapse rates. These lapse rates contributed to extreme instability with values of surface-based convective available potential energy exceeding 5000 J kg^{-1}. A closed upper-level low over the Northern Plains (not shown) was responsible for strong westerly winds of 25 m s^{-1} at 500 hPa. Through the afternoon hours, low-level shear increased as low-level winds intensified and became more southeasterly. Analysis of the 1 June 2015 0000 UTC Norman sounding—launched within two hours of tornadogenesis—showed strong directional and speed shear in the lowest three km (Fig. 1b). This shear resulted in values of 0–1 km storm relative helicity values just below 300 m^2 s^{-2}.

Shortly before 2130 UTC, storms developed near the intersection of a stationary surface front and the dryline (Fig. 2, 3a). The storms quickly intensified and NWS forecasters responded by issuing a severe thunderstorm warning at 2146 UTC (NWS Performance Management 2013; Fig. 3b). As the storm cluster continued to organize, it developed a low-level mesocyclone (not shown) and NWS forecasters issued the first tornado warning at 2236 UTC (NWS Performance Management; Fig. 3c). About 20 min later, the storm produced a weak tornado west of El Reno, OK at 2255 UTC (NCDC 2013). By 2257 UTC, the storm had a classic supercell appearance on radar (Fig. 3d). At 2303 UTC, the supercell (hereafter Supercell 1) produced a second tornado—the long-track "El Reno tornado"—that persisted until 2344 UTC and tragically claimed eight lives (NCDC 2013). A second supercell (hereafter Supercell 2) developed to the west of the primary supercell by 2327 UTC (Fig. 3e). It had much weaker low-level rotation and produced a brief EF0 tornado at 2355 UTC (NCDC 2013).

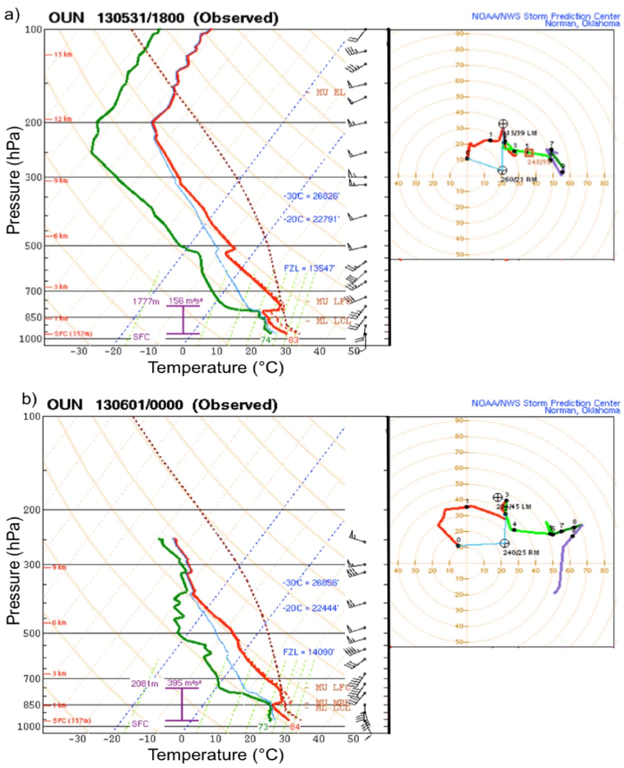

Fig. 1. Norman, Oklahoma soundings and hodographs for a) 1800 UTC 31 May 2013 and b) 0000 UTC 1 June 2013 obtained from the Storm Prediction Center's Severe Weather Events Archive. Red line is temperature and green line is dewpoint temperature. For more information about the content of these images see http://www.spc.noaa.gov/exper/soundings/help/index.html.

4. RADAR DATA ANALYIS AND RESULTS

To quantify magnitude and size of the Z_{DR} and K_{DP} column and the K_{DP} foot over time, we first identified each signature in KOUN data and manually extracted data from the Z, Z_{DR}, ρ_{hv}, and K_{DP} fields. To calculate magnitude, we took the mean of every range gate that met defined thresholds (e.g., Z_{DR} 2.0 dB or higher and ρ_{hv} 0.8 or higher) within each signature. To calculate size, we found the area of every range gate that met these defined thresholds and took the sum of these areas to find the signature's total size. To quantify overlap between the Z_{DR} and K_{DP} columns, we counted all gates where Z_{DR} was 1.0 dB and higher and K_{DP} was 1.0° km^{-1} and higher. We then calculated percent overlap by comparing this number with the combined number of gates comprising the Z_{DR} and K_{DP} columns. For the Z_{DR} arc, we found an average maximum by calculating the mean of nine range gates, which included the maximum value within the signature and all adjacent range gates (e.g., Mahale et al 2012). To quantify magnitude of the low-level mesocyclones, we used PAR data to calculate the maximum gate-to-gate velocity differential (delta V) over time. This calculation was performed at all elevation angles below three km ARL, but only the 0.5° elevation angle (i.e., closest to the surface) is presented to show low-level mesocyclone evolution.

We focused on dual-polarization signatures that may provide insight into updraft and downdraft evolution within the supercell and changes in the environmental wind shear. Z_{DR} columns provide information about updraft intensity while the K_{DP} column and K_{DP} foot may provide information about the storm's downdraft (e.g., Kumjian and Ryzhkov 2008; Kumjian et al. 2012). For example, Picca et al. (2010) observed a decrease in Z_{DR} column depth prior to multiple instances of tornadogenesis in three different cases. This decreasing Z_{DR} column depth may provide evidence of a weaker updraft associated with a divided mesocyclone and therefore potential tornadogenesis (e.g., Adlerman et al. 1999). It is also possible that Z_{DR} columns increase in size or magnitude prior to tornadogenesis as strong updrafts tilt and stretch horizontal vorticity (e.g., Wicker and Wilhelmson 1995; Davies-Jones et al. 2001). Kumjian et al. (2010) also noted that as Z_{DR} column size increased, K_{DP} column size decreased. It is therefore possible that patterns could exist in K_{DP} column evolution prior to tornadogenesis similar to patterns in Z_{DR} column evolution, but inversed. Additionally, changes in the Z_{DR} arc may indicate changes in the near-storm environmental wind shear, which could

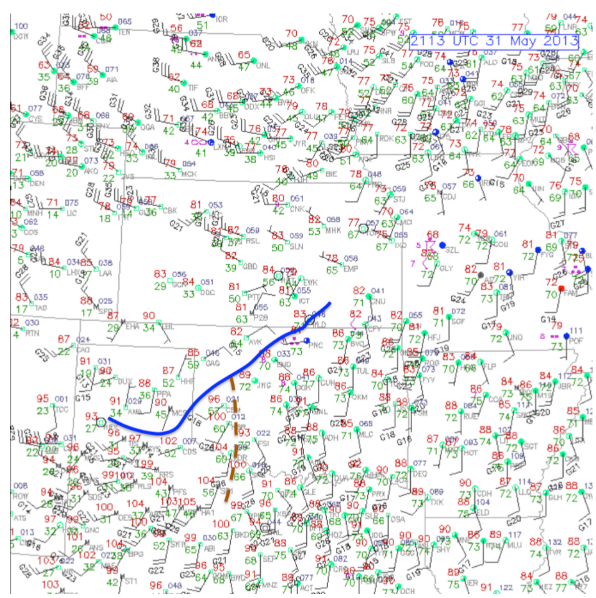

Fig. 2. Surface observations at 2113 UTC on 31 May 2013. Approximate location of the stationary front (blue) and dryline (dashed brown) are annotated. Station surface observations are temperature (°F, red), dewpoint temperature (°F, green), pressure (hPa, blue), and wind speed and direction (full barb=10 kt). Data from UCAR image archive, available
at http://www.mmm.ucar.edu/imagearchive/.

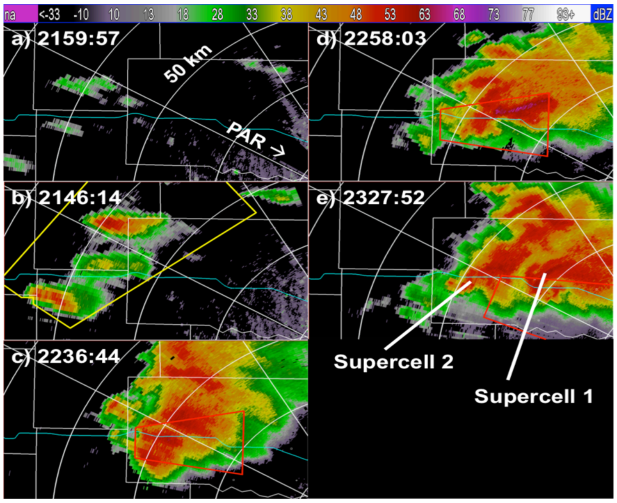

Fig. 3. PAR 0.5° reflectivity at a) 2159:57 UTC, b) 2146:14 UTC, c) 2236:44 UTC, and d) 2258:03 UTC and PAR 1.30° reflectivity at e) 2327:52 UTC on 31 May 2013. Reflectivity (dBZ) color bar located at the top. White rings are in 25 km increments. Severe thunderstorm warnings are outlined in yellow, and tornado warnings are outlined in red.

indicate an increase in a storm's tornado threat (e.g., Kumjian et al. 2010; Mahale et al. 2012). Therefore we compared the evolution of these signatures to low-level mesocyclone intensity to identify any potential tornadogenesis precursors that could aid forecasters in assessing tornado potential.

4.1 Z_{DR} RING/COLUMN

Both supercells had clear Z_{DR} columns that were distorted into ring or half-ring shapes by a mesocyclone. The Z_{DR} column of Supercell 1 exhibited multiple periods of increasing and decreasing magnitude and size during the life cycle of three—one nontornadic and two tornadic—mesocyclones (Fig. 4). The peaks (i.e., relative maxima in magnitude occurring at 2227:23, 2255:41, and 2337:08 UTC) did not appear to be clearly related to mesocyclone evolution in this study. A peak in magnitude and size occurred about 4.5 min prior to development of the first mesocyclone (nontornadic). After a period of decreasing magnitude and size, Z_{DR} column magnitude increased to another peak at 2255:41 UTC. This peak occurred at the same time as the second mesocyclone (tornadic) reached its maximum intensity and about six min prior to rapid intensification of the third mesocyclone (Fig. 4a). Z_{DR} column size also increased during this time, but did not reach a second peak until 2318:11 UTC, which was about 23 min after the second mesocyclone's maximum intensity and about 17.5 min after rapid intensification of the third mesocyclone (Fig. 4b).

As the third mesocyclone intensified and produced a strong (EF3) tornado, Z_{DR} column magnitude was variable, but did decrease by approximately 1.0 dB between 2312:16 and 2333:35 UTC. Z_{DR} column size also decreased to a relative minimum at the same time as mesocyclone maximum intensity at 2328:15 UTC. This decrease in Z_{DR} column size and magnitude may relate to a weakening updraft caused by the downward directed pressure gradient force induced by an intensifying mesocyclone (e.g., Rotunno and Klemp 1982). A weaker updraft could result in a weakening and shrinking Z_{DR} column (e.g., Picca et al. 2010, 2015). This hypothesis, however, does not explain the period of increasing Z_{DR} column magnitude (2303:59–2312:16 UTC) or the corresponding increase in Z_{DR} column size (2300:26–2318:11 UTC) as the mesocyclone intensified (Fig. 4). After reaching relative minima, Z_{DR} column magnitude and size increased dramatically as the third mesocyclone dissipated.

The Z_{DR} column associated with Supercell 2 was more constant (i.e., fewer maxima and minima in magnitude and size) than that with Supercell 1, but still had one peak in magnitude and two peaks in size (Fig. 5). The first peak in magnitude and size occurred at 2302:48 and 2307:46 UTC, respectively, and were not associated with low-level or midlevel mesocyclone development. A midlevel mesocyclone was present above 3.5 km by 2331 UTC, but it never organized near the surface. After reaching these peaks, magnitude decreased by about 1.5 dB and size decreased by about 65 km^2 by 2334:09 UTC. Magnitude then remained nearly constant through 0006:19 UTC, even as a low-level mesocyclone developed and produced a brief tornado (Fig. 5a). Z_{DR} column size did increase prior to mesocyclone development, however; and reached a relative maximum at the same time that the low-level mesocyclone developed (2353:13 UTC). The peak associated with low-level mesocyclone development was smaller than the peak that occurred earlier with no low-level mesocyclone development. In addition, peaks in Z_{DR} column and magnitude were observed with tornadic and nontornadic mesocyclones associated with Supercell 1. Therefore, it is challenging to comment on operational implications since Z_{DR} column magnitude and size did not appear to aid in discriminating between tornadic and nontornadic mesocyclones in this case.

Peaks in Z_{DR} column magnitude and size did occur prior to severe hail reports (Fig. 4). The first peak in magnitude occurred just after a report of 1.25-in hail, but the second peak occurred about 10 min prior to 5.90-in hail and the third peak occurred about eight min prior to 1.0-in hail (Fig. 4a; NCDC 2013). The Z_{DR} column evolution of Supercell 1 also appeared to be closely related to evolution of the upper-level reflectivity core, which is another operational indicator of updraft strength (Fig. 6). The relationship was not as clear with Supercell 2 (not shown).

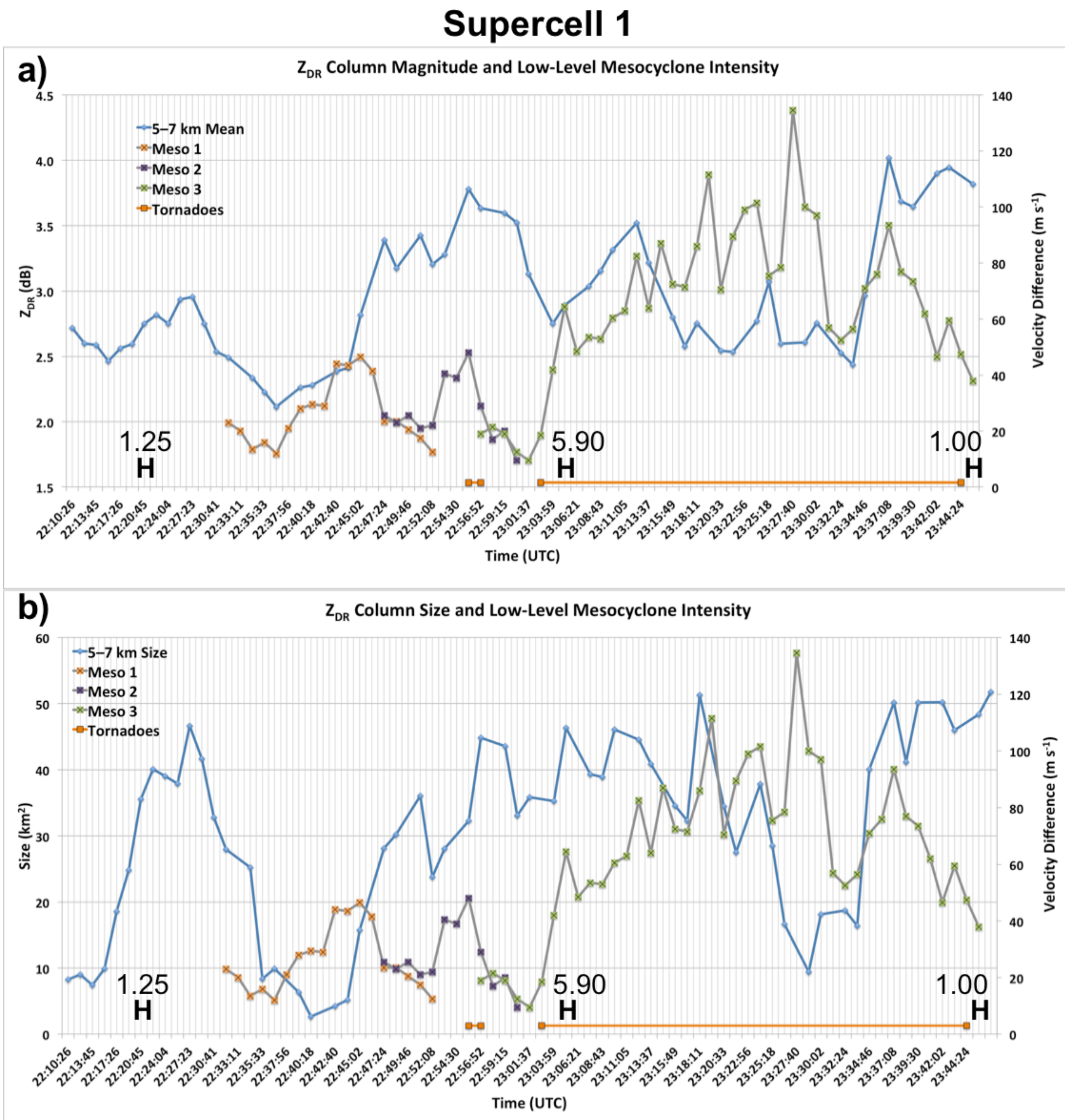

Fig. 4. Evolution of maximum gate-to-gate delta V at 0.5° for each mesocyclone and a) Z_{DR} column magnitude and b) Z_{DR} column size for Supercell 1. Solid grey lines with colored markers represent mesocyclone delta V and solid blue line represents Z_{DR} column magnitude (a) and size (b). The horizontal orange lines indicate when a tornado was ongoing. **H** indicates times of hail reports with numbers indicating corresponding size in inches.

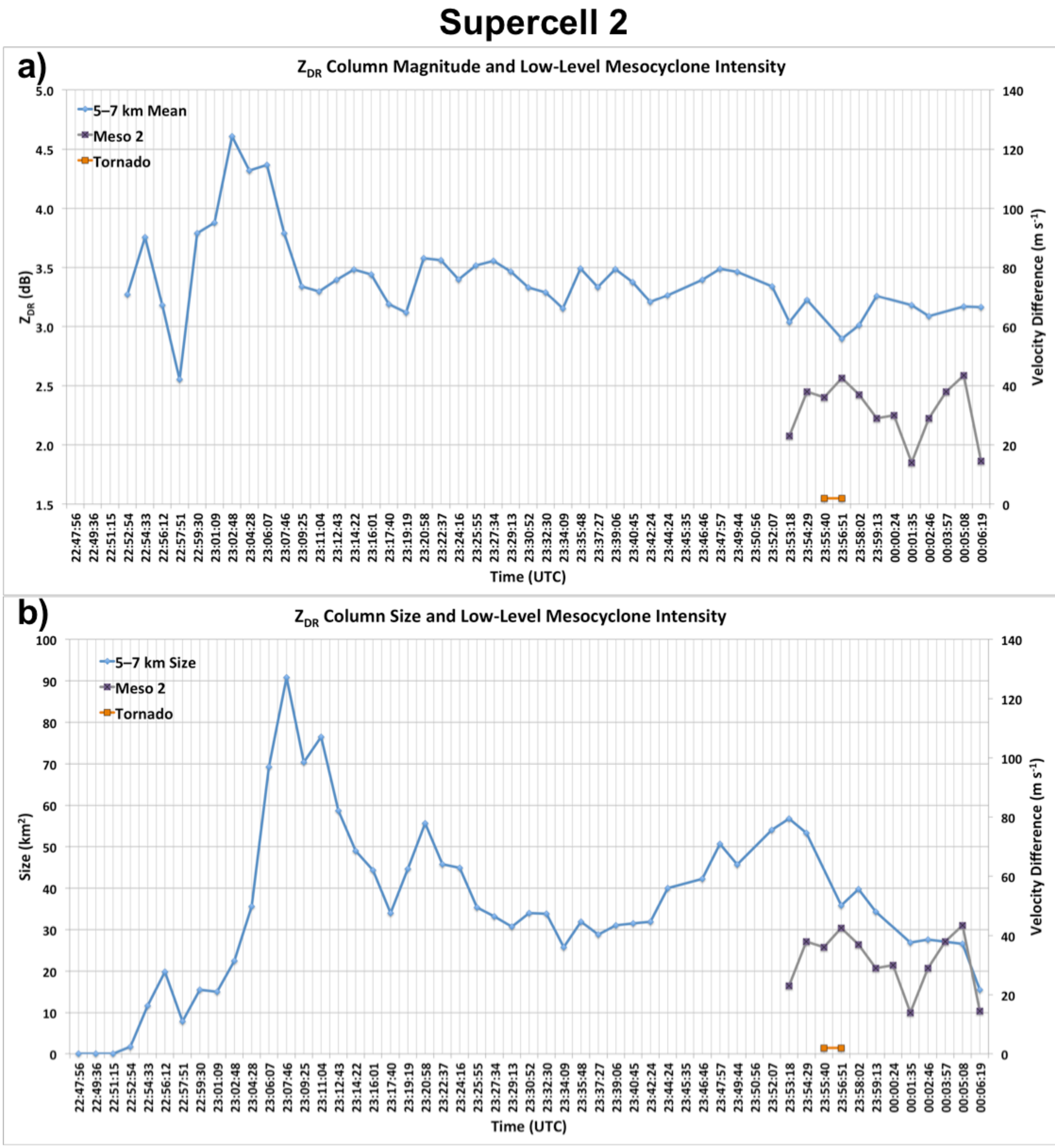

Fig. 5. Evolution of maximum gate-to-gate delta V at 0.5° for each mesocyclone and a) Z_{DR} column magnitude and b) Z_{DR} column size for Supercell 2. Solid grey line with dark markers represents mesocyclone delta V and solid blue line represents Z_{DR} column magnitude (a) and size (b). The horizontal orange line indicates when a tornado was ongoing.

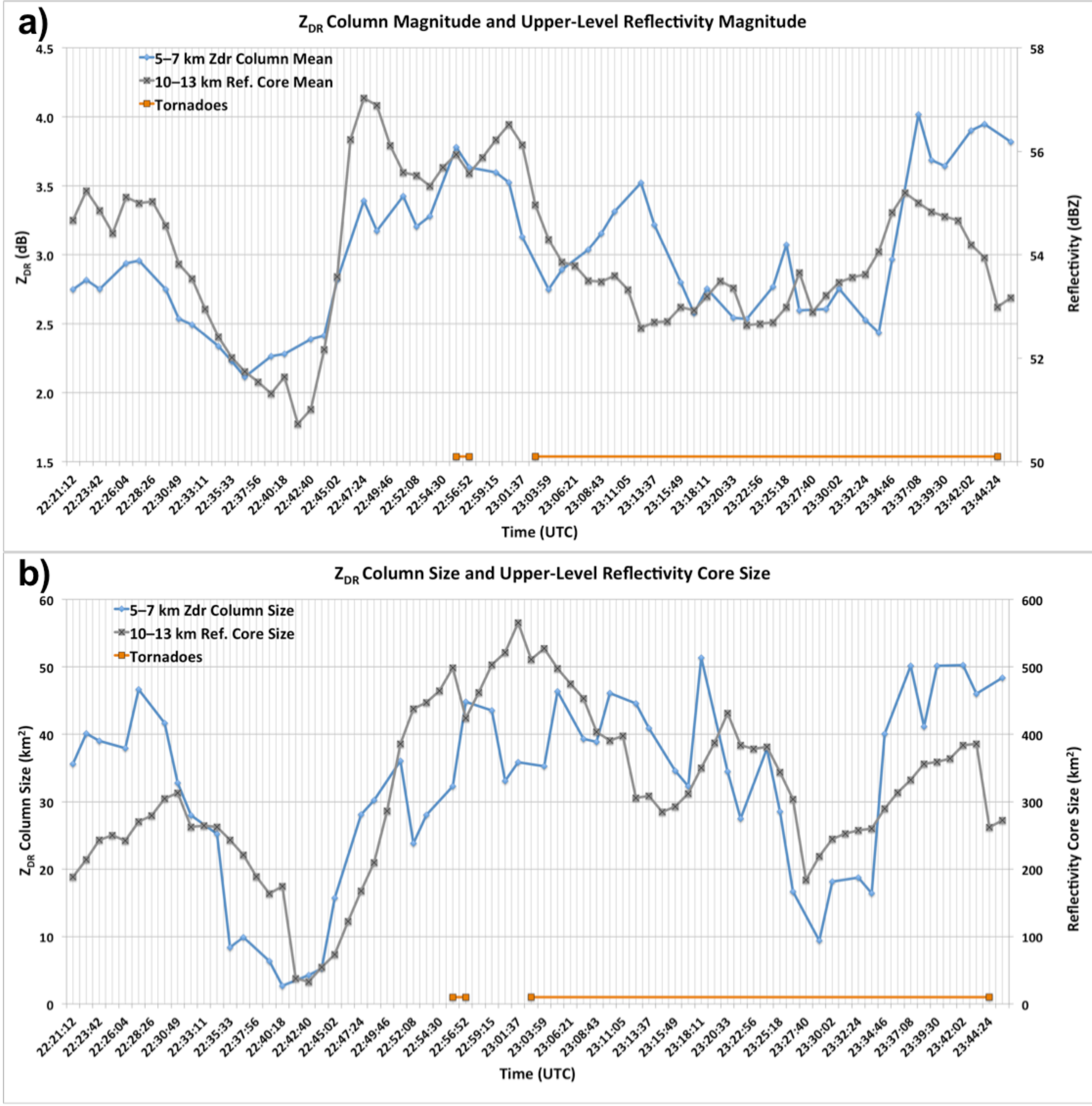

Fig. 6. Evolution of a) Z_{DR} column and upper-level reflectivity core magnitude and b) Z_{DR} column and upper-level reflectivity core size for Supercell 1. The horizontal orange line indicates when a tornado was ongoing. Solid grey (blue) line represents upper-level reflectivity core (Z_{DR} column) magnitude (a) and size (b).

4.2 K_{DP} COLUMN

Both supercells also contained well-defined K_{DP} columns. The K_{DP} column of Supercell 1 evolved in a manner that appeared independent of the three analyzed mesocyclones. Size and magnitude generally increased between 2210:26 and 2253:19 UTC as the first mesocyclone completed its life cycle and the second mesocyclone developed and intensified (Fig. 7). No clear differences appeared in the evolution of K_{DP} column magnitude and size relative to the intensity of these mesocyclones despite one being nontornadic and the other two tornadic. After reaching peak magnitude and intensity at 2248:35 and 2253:19 UTC respectively, the K_{DP} column generally weakened and shrank as the second mesocyclone produced a weak tornado and the third mesocyclone rapidly intensified and produced a tornado. After decreasing, K_{DP} column magnitude remained fairly steady through 2337:08 UTC. It then steadily increased after 2337:08 UTC as the third mesocyclone dissipated (Fig. 7a). K_{DP}

column size was relatively variable during this time (2308:43–2345:35 UTC) and did not appear to relate to mesocyclone evolution (Fig. 7b).

The K_{DP} column of Supercell 2 was more constant than the K_{DP} column of Supercell 1, especially with respect to magnitude. The magnitude remained relatively steady through the entire analysis period and did not provide any clear signal prior to low-level mesocyclogenesis or tornadogenesis (Fig. 8a). Analysis of K_{DP} column size revealed two distinct peaks (Fig. 8b). One occurred without the presence of a low-level mesocyclone and the other occurred prior to the development of a tornadic low-level mesocyclone. The maximum K_{DP} column size occurred about five min prior to low-level mesocyclone development and about seven min prior to tornadogenesis. Size then generally decreased from 48.0 km^2 to 7.9 km^2 over the next 18 min as mesocyclone intensity remained relatively constant.

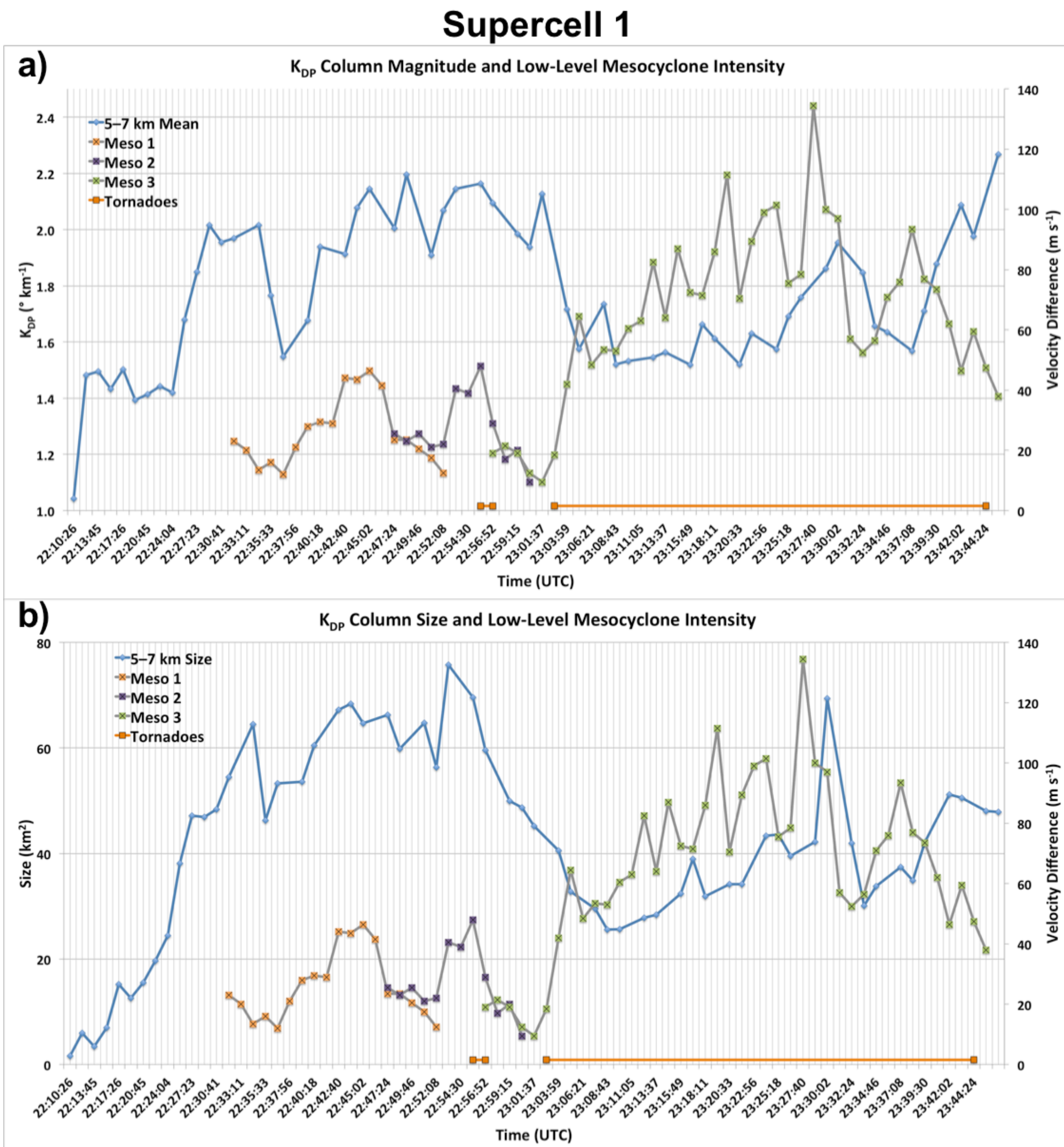

Fig. 7. Evolution of maximum gate-to-gate delta V at 0.5° for each mesocyclone and a) K_{DP} column magnitude and b) K_{DP} column size for Supercell 1. Solid grey line with colored markers represents mesocyclone delta V and solid blue line represents K_{DP} column magnitude (a) and size (b). The horizontal orange line indicates when a tornado was ongoing.

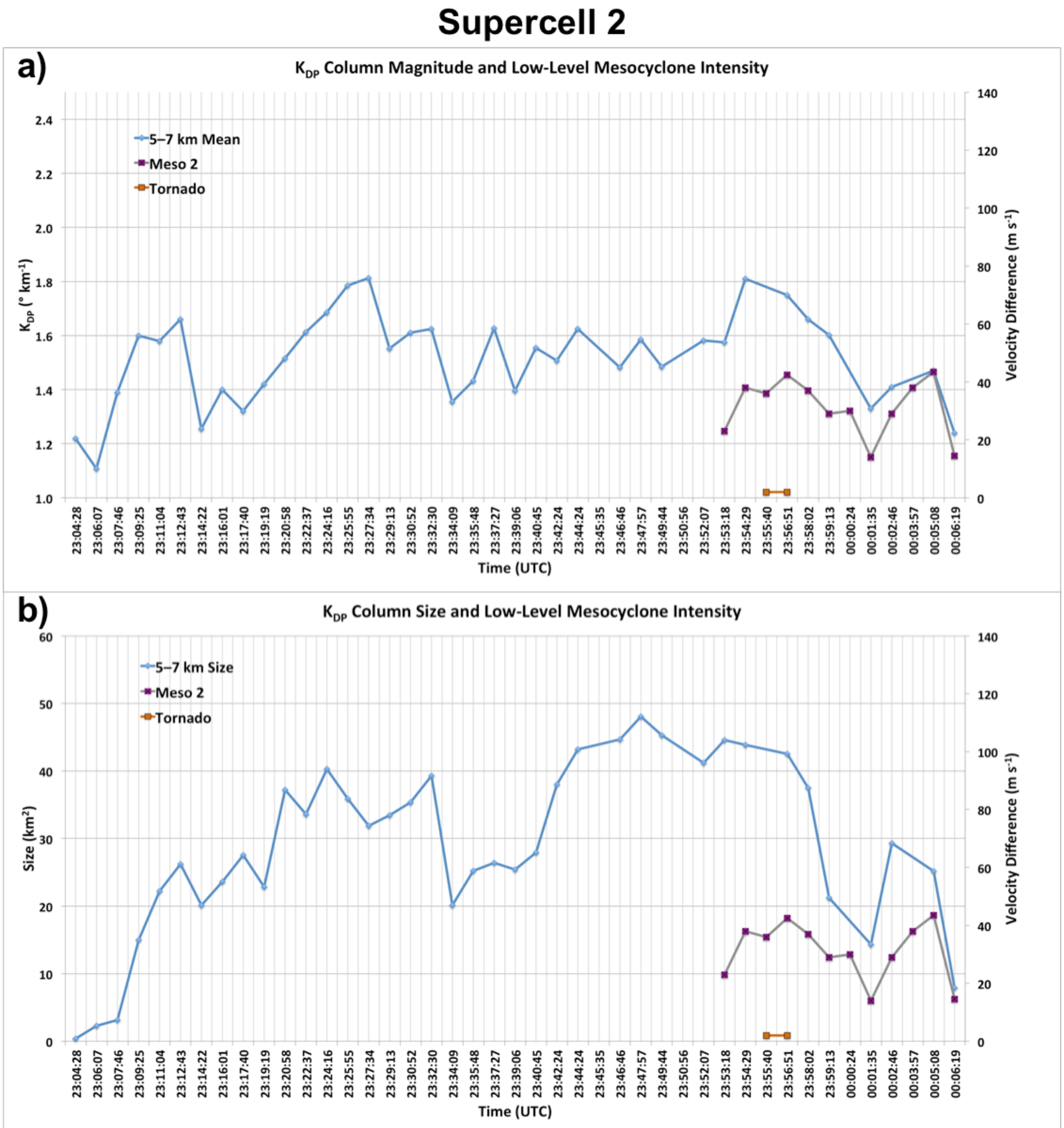

Fig. 8. Evolution of maximum gate-to-gate delta V at 0.5° for each mesocyclone and a) K_{DP} column magnitude and b) K_{DP} column size for Supercell 2. Solid grey line with dark markers represents mesocyclone delta V and solid blue line represents K_{DP} column magnitude (a) and size (b). The horizontal orange line indicates when a tornado was ongoing.

4.3 Z_{DR} ARC

Both supercells contained a Z_{DR} arc, though the Z_{DR} arc with Supercell 1 was more defined, had a more obvious arc shape (Fig. 9), and lasted longer. The Z_{DR} arc with Supercell 1 first developed at 2246:13 UTC. Its evolution contained several peaks during the life cycle of two tornadic mesocyclones (Fig. 10a). The first two peaks occurred at 2253:19 and 2301:37 UTC and were both observed approximately 1.5 min prior to tornadogenesis. Two later peaks—one at 2314:38 UTC and the other at 2324:07 UTC—also occurred approximately three min prior to relative maxima in mesocyclone intensity. Later, as the mesocyclone intensity decreased, so did Z_{DR} arc magnitude (Fig. 10).

The Z_{DR} arc associated with Supercell 2 had three peaks (Fig. 10b). The first two peaks occurred at 2340:45 and 2349:44 UTC and did not appear to be associated with low-level mesocyclone development or tornadogenesis. The second peak did occur approximately 3.5 min prior to low-level mesocyclogenesis and six min prior to tornadogenesis, however. After the first two peaks, the largest peak occurred at 2355:40 UTC or at approximately the same time as tornadogenesis (Fig. 10b).

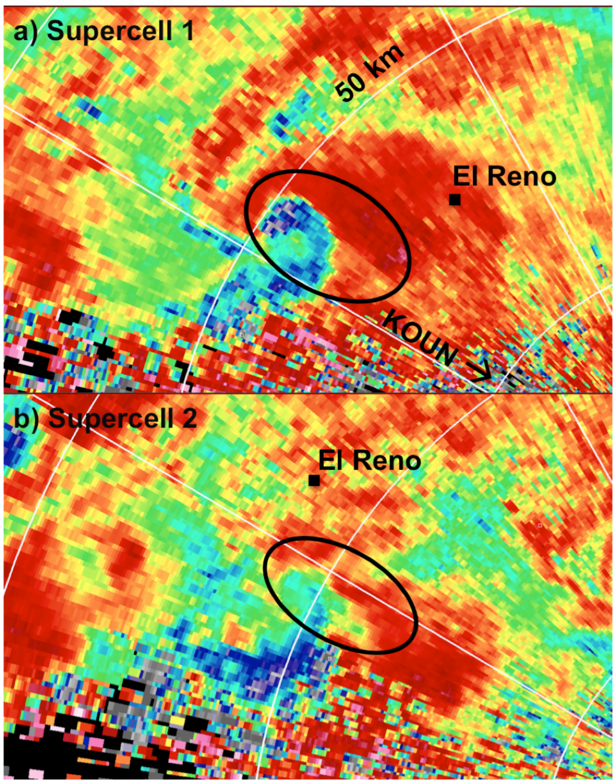

Fig. 9. 0.5° Z_{DR} field showing the Z_{DR} arc for a) Supercell 1 at 2324:16 UTC on 31 May 2013 and b) Supercell 2 at 0000:30 UTC on 1 June 2013. Black circles indicate approximate location of Z_{DR} arcs. White rings are in 25 km increments.

4.4 K_{DP} FOOT

Both supercells contained a well-defined K_{DP} foot. K_{DP} foot magnitude and size of Supercell 1 did not appear to be affected by mesocyclone evolution. No clear trends were observed in magnitude from 2214:28–2307:32 UTC as mean K_{DP} values fluctuated between 2.7 and 3.3° km^{-1} (Fig. 11a). During the same time, K_{DP} foot size reached two relative maxima. They occurred 23.5 and 3.5 min prior to the maximum intensity of the first mesocyclone and 34 and 14 min prior to the maximum intensity of the second mesocyclone (Fig. 11b). It is unclear whether these peaks in size were related to the evolution of either the first or second mesocyclone. Hereafter, beginning at 2258:03 UTC, K_{DP} foot size increased dramatically from 91.5 km^2 at 2258:03 UTC to 203.9 km^2 at 2309:54 UTC. This increasing trend occurred as the third mesocyclone developed, rapidly intensified, and produced a strong tornado (Fig. 11b). The increasing trend began five min prior to tornadogenesis and the maximum size occurred seven min after tornadogenesis. Therefore, the largest change in K_{DP} foot size would likely have given forecasters little lead time in anticipating mesocyclone intensification or tornadogenesis in this case. After this peak in size, K_{DP} foot magnitude and size generally decreased through 2320:33 UTC as the third mesocyclone continued to intensify (Fig. 11). They both then increased as mesocyclone intensity generally decreased through 2345:35 UTC.

K_{DP} foot magnitude of Supercell 2 was relatively constant while size generally increased (Fig. 12). Magnitude only fluctuated between 2.1 and 3.1° km^{-1} and did not have any clear relative maxima (Fig. 12a). The maximum magnitude occurred at 0007:40 UTC (1 June 2013), or approximately 12.5 min after tornadogenesis. During approximately the same time (2309:25–0005:08 UTC), K_{DP} foot size increased by 211 km^2 and reached its maximum at 0005:08 UTC or about one min prior to mesocyclone dissipation and 10 min after tornadogenesis. We observed no clear precursors to tornadogenesis in K_{DP} foot size.

4.5 Z_{DR} AND K_{DP} COLUMN OVERLAP

Our analysis revealed no clear patterns in Z_{DR} and K_{DP} column overlap relative to low-level mesocyclone intensity or tornadogenesis (Fig. 13). For Supercell 1, percent overlap reached a maximum value of 58.1% at 2234:22 UTC as the first mesocyclone developed (Fig. 13a). It then decreased and remained below 50% between 2240:18 and 2339:30 UTC as the first two mesocyclones intensified and dissipated and the third mesocyclone reached maximum intensity. Percent overlap did briefly rise above 50% once again at 2342:02 UTC or about 3.5 min prior to the third mesocyclone's dissipation. In Supercell 2, percent overlap was fairly steady and always remained below 50% (Fig. 13b). No clear patterns existed prior to low-level mesocyclone development or tornadogenesis.

This result adds evidence to the results of previous studies that observed a minimal amount of overlap between the Z_{DR} and K_{DP} columns of supercells (e.g., Loney et al. 2002; Kumjian and Ryzhkov 2008). In this case, the percent overlap was frequently below 50% for both supercells and averaged 33% for Supercell 1 and 28% for Supercell 2.

5. OPERATIONAL RELEVANCE

Any information that can increase NWS forecaster ability to anticipate upcoming storm threats adds

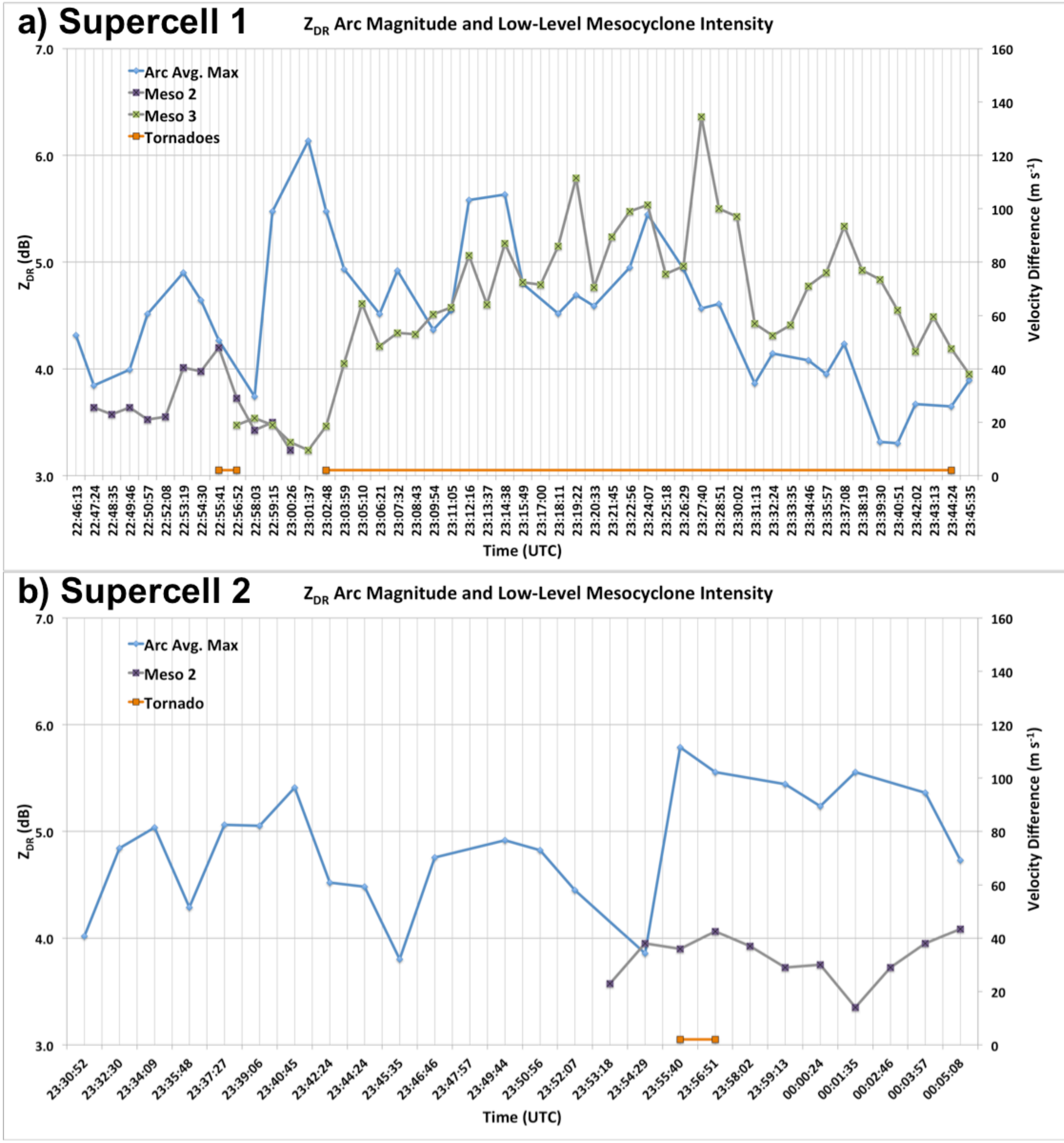

Fig. 10. Evolution of maximum gate-to-gate delta V at 0.5° for each mesocyclone and Z_{DR} arc magnitude for a) Supercell 1 and b) Supercell 2. Solid grey lines with colored markers represent mesocyclone delta V and solid blue line represents Z_{DR} arc magnitude. The horizontal orange line indicates when a tornado was ongoing.

value to the warning process (Andra et al. 2002). In this case, we searched for potential tornadogenesis precursors in the evolution of four dual-polarization supercell signatures. Our analysis revealed evolutionary trends and patterns, though none of them appeared to provide signals for tornadogenesis or aid in discriminating between tornadic and nontornadic mesocyclones. For the Z_{DR} column, K_{DP} column, and K_{DP} foot, peaks in magnitude and size either occurred prior to or concurrently with tornadic and nontornadic mesocyclones or they did not appear to have any relationship to mesocyclone evolution (Fig. 4, 5, 7, 8, 11–12). Additionally, the first peak in Z_{DR} and K_{DP} column magnitude and size of Supercell 2 were not associated with low-level mesocyclogenesis (i.e., false positive). We also compared these signatures to each other (e.g., Z_{DR} column shape; distance between the Z_{DR} arc and K_{DP} foot maximum) and with inflow evolution, but found no clear differences between tornadic and nontornadic mesocyclones or precursors to tornadogenesis. These results are consistent with previous studies that did not find a clear difference between the dual-polarization signatures of tornadic and nontornadic supercells (e.g., Kumjian and Ryzhkov 2008; Kumjian 2013). Without clear and consistent evolutionary patterns associated with tornadic and nontornadic mesocyclones, it could be difficult for a forecaster to use these signatures to increase confidence in issuing or not issuing a tornado warning, at least in this case. More quantitative studies are needed to address potential operational uses of dual-polarization signatures during the tornado-warning process.

Potential tornadogenesis signals did appear in Z_{DR} arc magnitude for both supercells considered. In Supercell 1, sharp peaks in Z_{DR} arc magnitude occurred approximately 1.5–3.0 min prior to tornadogenesis or increases in mesocyclone intensity (Fig. 10a). In Supercell 2, a peak occurred at approximately the same time as tornadogenesis (Fig. 10b). Peaks also occurred without tornadogenesis in Supercell 2, however. The presence of these false positives with Supercell 2 and peaks occurring so close in time to tornadogenesis with both supercells likely limits the usefulness of this signature in terms of issuing tornado warnings, at least in this case. For example, the forecaster who issued warnings in real time for this case issued the first tornado warning 17 min prior to these peaks in Z_{DR} arc magnitude using reflectivity, velocity, and environmental data (Kuster et al. 2015).

Despite a lack of tornadogenesis precursors observed here, previous research has identified some operational uses for dual-polarization supercell signatures. The development of a Z_{DR} arc or Z_{DR} ring can occur prior to low-level mesocyclone development and could therefore alert a forecaster than a given storm or is transitioning from a multicell to a supercell (e.g., Romine et al. 2008; Kumjian 2013). In a QLCS, development of a Z_{DR} arc or separation between the Z_{DR} arc and K_{DP} foot could indicate that a given portion of the line poses a greater tornado threat (e.g., Mahale et al. 2012; Crowe et al. 2012). Growth of the Z_{DR} column—indicative of increasing updraft strength—can also provide a precursor for hail at the surface (e.g., Picca et al. 2010; Kumjian et al. 2012). This pattern also emerged in this case as peaks in Z_{DR} column magnitude and size preceded large hail reports by 8–10 min with Supercell 1 (Fig. 4). There were no hail reports with Supercell 2, but the storm did occur over mainly rural areas.

Acknowledgements. We thank Jeff Brogden, Karen Cooper, and Robert Toomey for their help with WDSSII and SOLO, Patrick Skinner for helping with radar data editing, and Emma Kuster and Tim Supinie for assistance with Python. Funding for the lead author was provided by NOAA/Office of Oceanic and Atmospheric Research under NOAA-University of Oklahoma Cooperative Agreement #NA11OAR4320072, U.S. Department of Commerce.

REFERENCES

Adlerman, E. J., K. K. Droegemeir, and R. Davies-Jones, 1999: A Numerical Simulation of Cyclic Mesocyclogenesis. *J. Atmos. Sci.*, **56**, 2045–2069.

Andra, D. L., E. M. Quoetone, and W. F. Bunting, 2002: Warning decision making: The relative roles of conceptual models, tech- nology, strategy, and forecaster expertise on 3 May 1999. *Wea. Forecasting*, **17**, 559–566.

Brown, R. A., B. A. Flickinger, E. Forren, D. M. Schultz, D. Sirmans, P. L. Spencer, V. T. Wood, and C. L. Ziegler, 2005: Improved detection of severe storms using experimental fine-resolution WSR- 88D measurements. *Wea. Forecasting*, **20**, 3–14.

Conway, J. W., and D. S. Zrnić, 1993: A study of embryo production of hail growth using dual-Doppler and multiparameter radar. *Mon. Wea. Rev.*, **121**, 2511–2528.

Crowe, C. C., C. J. Schultz, M. Kumjian, L. D. Carey, and W. A. Petersen, 2012: Use of dual-polarization signatures in diagnosing tornadic potential. *Electronic J. Operational Meteor.*, **13**, 57–78.

Davies-Jones, R. P., R. J. Trapp, and H. B. Bluestein, 2001: Tornadoes and tornadic storms. *Severe Convective Storms Meteor. Monogr.*, No. 50. Amer. Meteor. Soc., 167–221.

Dawson, D. T., E. R. Mansell, and M. R. Kumjian, 2015: Does wind shear cause hydrometeor size sorting? *J. Atmos. Sci.*, **72**, 340–348.

Doswell, C. A., III, and D. W. Burgess, 1993: Tornadoes and tornadic storms: A review of conceptual models. *The Tornado: Its Structure, Dynamics, Prediction, and Hazards, Geophys. Monogr.*, Vol. 79, Amer. Geophys. Union, 161–172.

Hubbert, J., V. N. Bringi, L. D. Carey, and S. Bolen, 1998: CSU-CHILL polarimetric radar measurements from a severe hail storm in eastern Colorado. *J. Appl. Meteor.*, **37**, 749–775.

Kumjian, M. R., 2013: Principles and applications of dual-polarization weather radar. Part II: Warm- and cold-season applications. *J. Operational Meteor.*, **1**, 243–264.

——, and A. V. Ryzhkov, 2008: Polarimetric signatures in supercell thunderstorms. *J. Appl. Meteor. Climatol.*, **47**, 1940–1961.

——, A. V. Ryzhkov, V. M. Melnikov, and T. J. Schuur, 2010: Rapid-scan super-resolution observations of a cyclic supercell with a dual-polarization WSR-88D. *Mon. Wea. Rev.*, **138**, 3762–3786.

——, S. M. Ganson, and A. V. Ryzhkov, 2012: Freezing in deep convective updrafts: A microphysical and polarimetric model. *J. Atmos. Sci.*, **69**, 3471–3490.

Kuster, C. M., P. L. Heinselman, and M. Austin, 2015: 31 May 2013 El Reno tornadoes: Advantages of rapid-scan phased-array radar data from a warning forecaster's perspective. *Wea. Forecasting*, **30**, 933–956.

Loney, M. L., D. S. Zrnić, J. M. Straka, and A. V. Ryzhkov, 2002: Enhanced polarimetric radar signatures above the melting level in a supercell storm. *J. Appl. Meteor.*, **41**, 1179–1194.

Mahale, V. N., J. A. Brotzge, and H. B. Bluestein, 2012: An analysis of vorticies embedded within a quasi-linear convective system using X-band polarimetric radar. *Wea. Forecasting*, **27**, 1520–1537.

NCDC, 2013: Storm events database. Accessed 1 September 2015. [Available online at http://www.ncdc.noaa.gov/stormevents/listevents.jsp?eventType5%28C%291Tornado&beginDate_mm505&beginDate_dd531&beginDate_yyyy52013&endDate_mm506&endDate_dd501&endDate_yyyy52013&county5ALL&hailfilter50.00&tornfilter50&windfilter5000&sort5DT&submitbutton5Search&statefips540%2COKLAHOMA.].

NOAA, 2013: Dual-polarization radar: Stepping stones to building a Weather-Ready Nation. Accessed 30 September 2015. [Available online at http://www.nws.noaa.gov/com/weatherreadynation/news/130425_dualpol.html#.VhaC3Le-1f5].

NWS Performance Management, 2013. Accessed 1 September 2013. [Available online at https://verification.nws.noaa.gov.].

Picca, J. C., M. Kumjian, and A. V. Ryzhkov, 2010: Z_{DR} columns as a predictive tool for hail growth and storm evolution. *Extended Abstracts, 25th Conf. on Severe Local Storms*, Denver, CO, Amer. Meteor. Soc., 11.3 [Available online at https://ams.confex.com/ams/pdfpapers/175750.pdf].

——, J. C. Snyder, and A. V. Ryzhkov, 2015: An observational analysis of Z_{DR} column trends in tornadic supercells. *Extended Abstracts, 37th Conf. on Radar Meteorology*, Norman, OK, Amer. Meteor. Soc., 5A.5. [Available online at https://ams.confex.com/ams/37RADAR/webprogram/Paper275416.html].

Romine, G. S., D. W. Burgess, and R. B. Wilhelmson, 2008: A dual-polarization-radar-based assessment of the 8 May 2003 Oklahoma City area tornadic supercell. *Mon. Wea. Rev.*, **136**, 2849–2870.

Rotunno, R. and J. B. Klemp, 1982: The influence of the shear-induced pressure gradient on thunderstorm motion. *Mon. Wea. Rev.*, **110**, 136–151.

Van Den Broeke, M. S., J. M. Straka, and E. N. Rasmussen, 2008: Polarimetric radar observations at low levels during tornado life cycles in a small sample of classic southern plains supercells. *J. Appl. Meteor. Climatol.*, **47**, 1232–1247.

Wakimoto, R. M, and V. N. Bringi, 1988: Dual-polarization observations of microbursts associated with intense convection: The 20 July storm during the MIST project. *Mon. Wea. Rev.*, **116**, 1521–1539.

Wicker, L. J., and R. B. Wilhelmson, 1995: Simulation and analysis of tornado development and decay within a three-dimensional supercell thunderstorm. *J. Atmos. Sci.*, **52**, 2675–2703.

Zrnić, D. S., V. N. Bringi, N. Balakrishnan, K. Aydin, V. Chandrasekar, and J. Hubbert, 1993: Polarimetric measurements in a severe hailstorm. *Mon. Wea. Rev.*, **121**, 2223–2238.

Characteristics	KOUN	PAR
Wavelength	11.09 cm	9.38 cm
Transmit Beamwidth	1.06°	1.5° at bore site, 2.1° at ±45°
Polarization	Dual-Polarization	Vertical
Elevation Angles (degrees)	0.52, 0.97, 1.50, 2.05, 3.05, 4.05, 5.05, 5.95, 7.97, 9.90	0.50, 0.90, 1.30, 1.80, 2.40, 3.10, 4.00, 5.10, 6.40, 8.00, 10.00, 12.50, 15.60, 19.50, 23.40, 28.20, 34.20, 42.80, 52.90
Volumetric Update Time	1.6 min (90° sector)	1.16 min (90° sector)

Table 1. Basic characteristics of KOUN and PAR on 31 May 2013.

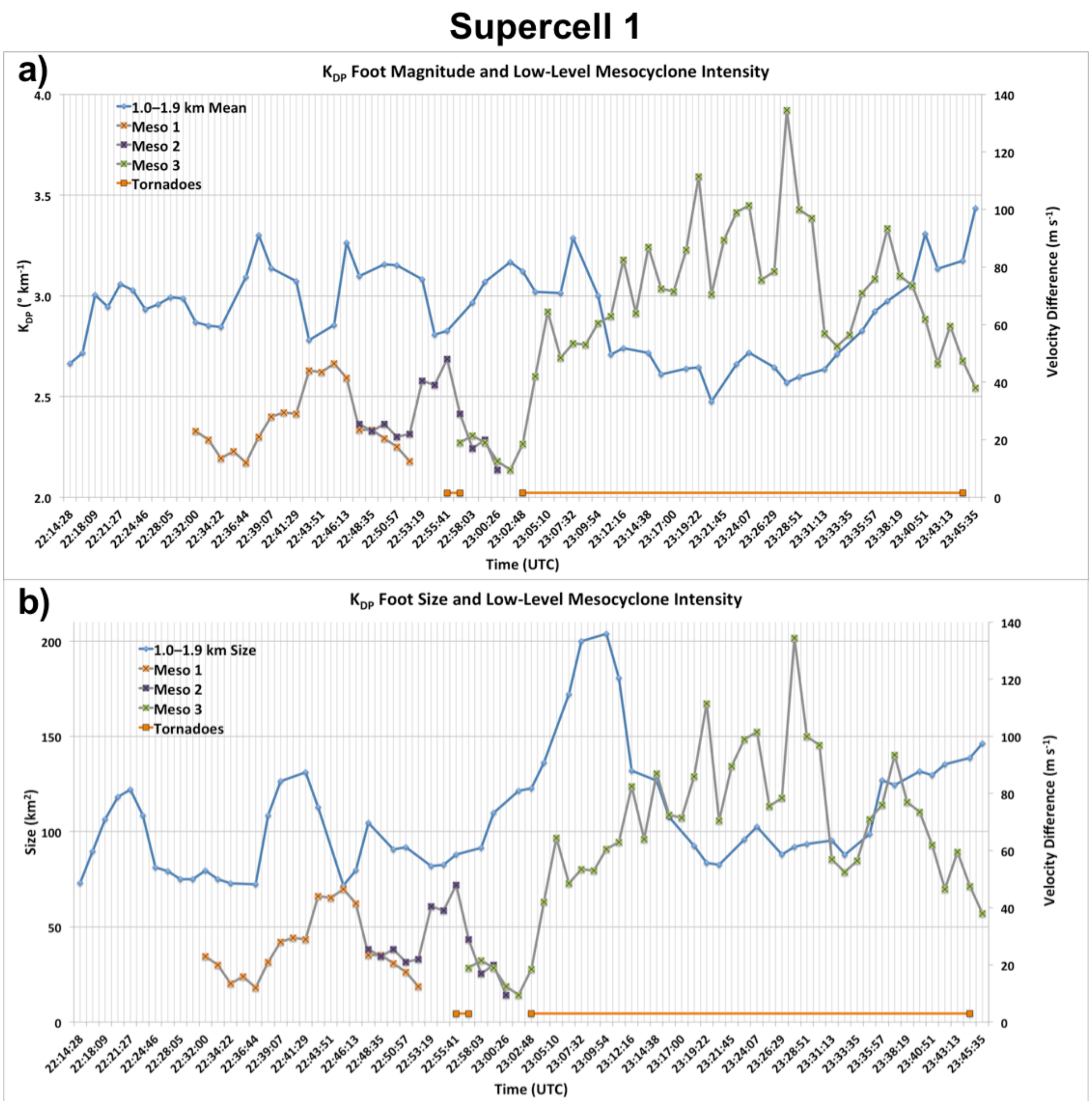

Fig. 11. Evolution of maximum gate-to-gate delta V at 0.5° for each mesocyclone and a) K_{DP} foot magnitude and b) K_{DP} foot size for Supercell 1. Solid grey line with colored markers represents mesocyclone delta V and solid blue line represents K_{DP} column magnitude (a) and size (b). The horizontal orange line indicates when a tornado was ongoing.

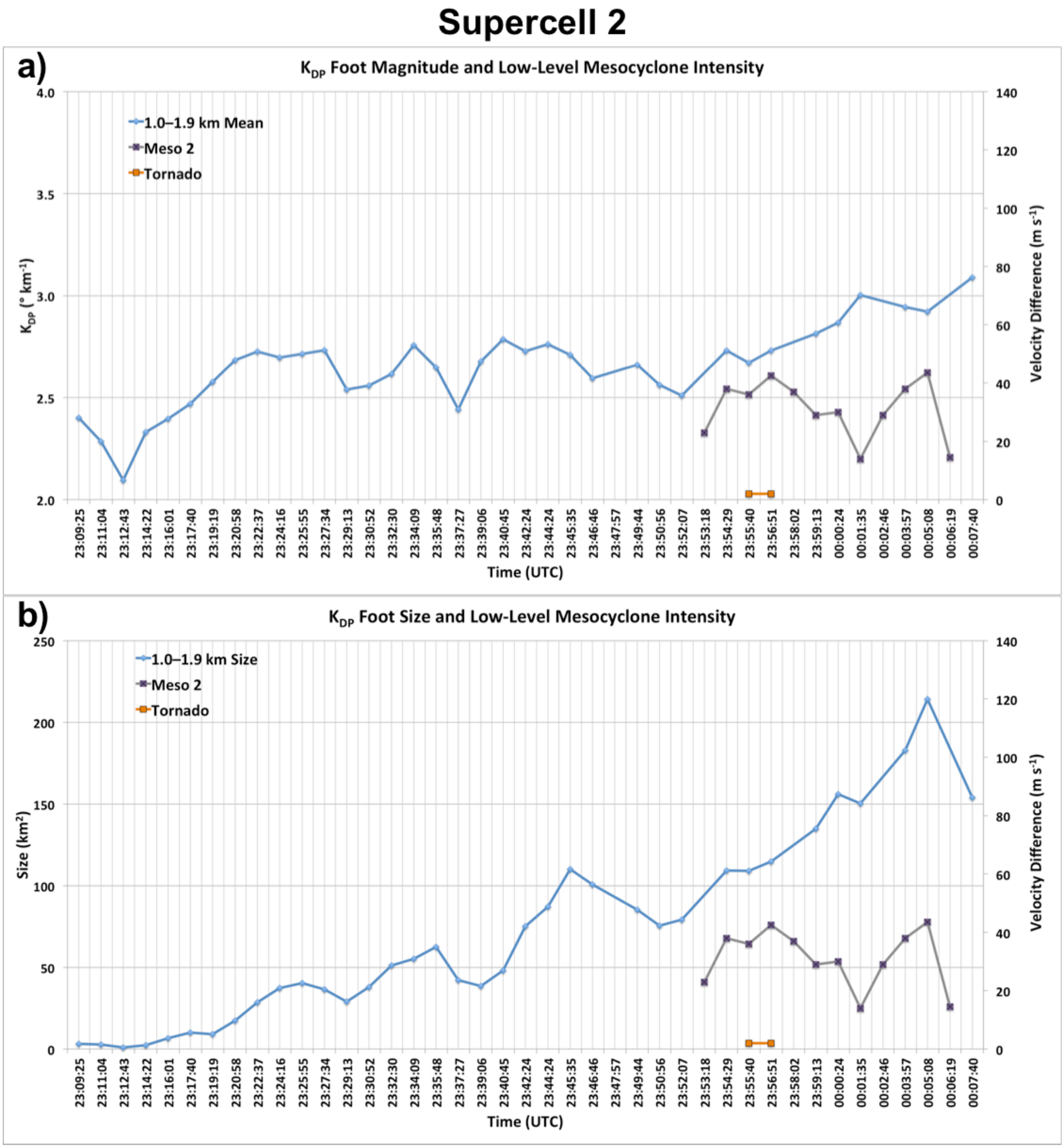

Fig. 12. Evolution of maximum gate-to-gate delta V at 0.5° for each mesocyclone and a) K_{DP} foot magnitude and b) K_{DP} foot size for Supercell 2. Solid grey line with dark markers represents mesocyclone delta V and solid blue line represents K_{DP} column magnitude (a) and size (b). The horizontal orange line indicates when a tornado was ongoing.

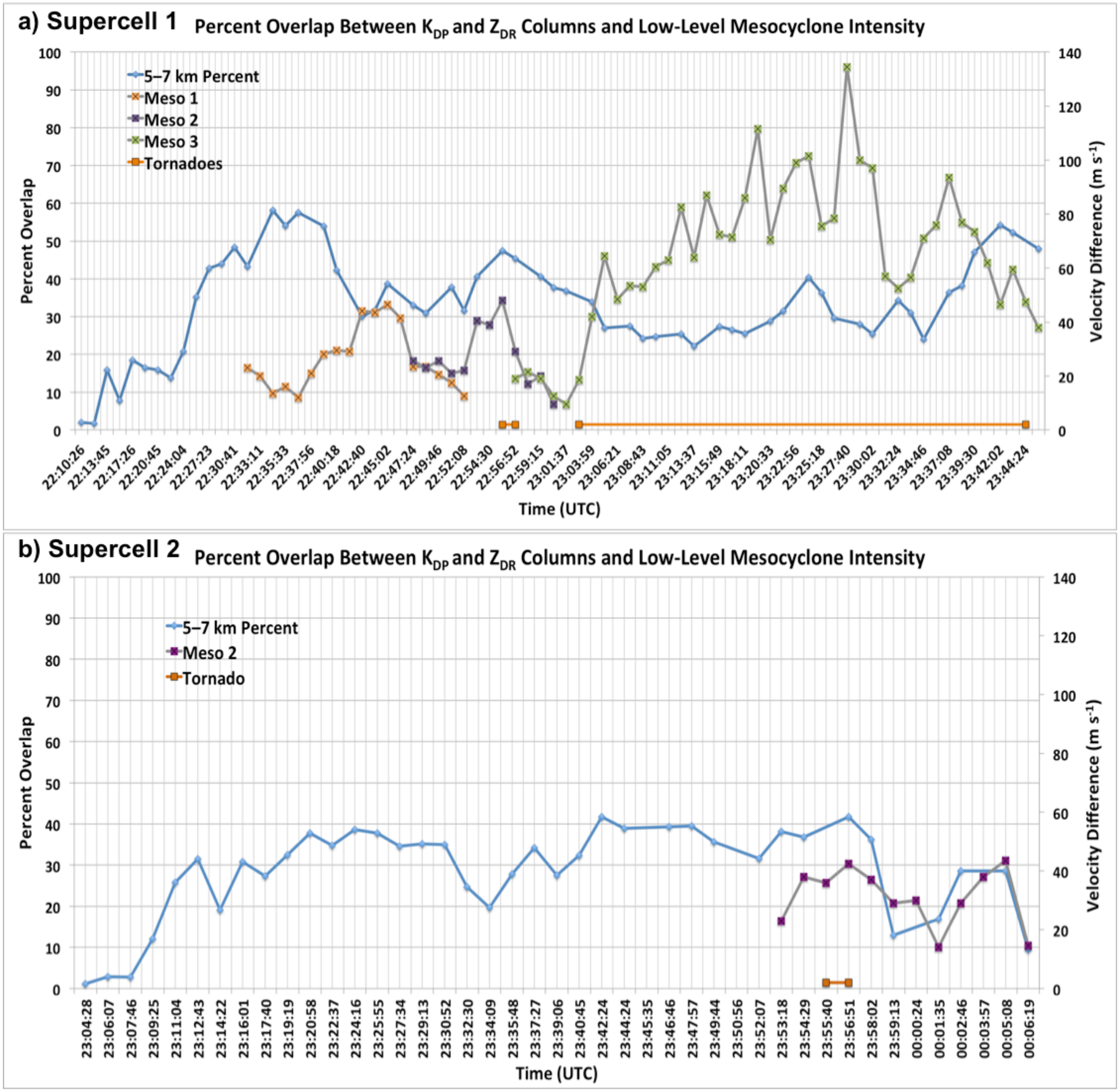

Fig. 13. Evolution of maximum gate-to-gate delta V at 0.5° for each mesocyclone and percent of overlapping radar gates between the Z_{DR} and K_{DP} columns for a) Supercell 1 and b) Supercell 2. Solid grey lines with colored markers represent mesocyclone delta V and solid blue line represents percent overlap. The horizontal orange line indicates when a tornado was ongoing.